

Modeling Neutron Star Atmospheres

V.E. Zavlin¹ and G.G. Pavlov²

¹ Max-Planck-Institut für extraterrestrische Physik, Giessenbachstraße, 85748 Garching, Germany

² The Pennsylvania State University, 525 Davey Lab, University Park, PA 16802, USA

Abstract. Models of thermal emission of neutron stars, presumably formed in their atmospheres, are needed to infer the surface temperatures, magnetic fields, chemical composition, and neutron star masses and radii from the observational data. This information, supplemented with model equations of state and neutron star cooling models, is expected to move us further in understanding the fundamental properties of the superdense matter in the neutron star interiors. The neutron star atmospheres are very different from those of usual stars due to the immense gravity and huge magnetic fields. In this presentation we review the current status of the neutron star atmosphere modeling and present most important results.

1. Introduction

A systematic study of X-ray emission from isolated neutron stars (NSs), including radio pulsars, has started after the launch of the *Einstein* and *EXOSAT* space observatories. These studies have shown that, generally, there are two different components of the NS X-ray emission — thermal and nonthermal. The nonthermal component with a power-law spectrum, observed from many radio pulsars, is believed to originate from the pulsar’s magnetosphere, while the thermal component is emitted from the NS surface layers (atmospheres). The thermal radiation is particularly interesting because it can provide important information about the NS: its surface temperature, magnetic field, and chemical composition, as well as the NS radius and mass. Measuring these parameters for a sample of NSs is necessary for studying the thermal evolution of NSs and constraining the equation of state and composition of the superdense matter in the NS interiors (see the review by Yakovlev et al. in these Proceedings).

Thermal X-ray emission from the NS surface had been discussed by Chiu & Salpeter and Tsuruta in 1964, before NSs were discovered, and well before their thermal emission was detected with *Einstein* and *EXOSAT* (e.g., Cheng & Helfand 1983; Brinkmann & Ögelman 1987; Córdoba et al. 1989; Kellet et al. 1987). Many new observational results on the NS thermal radiation were obtained in 1990’

with the *ROSAT*, *ASCA*, and *EUVE* satellites (see Becker & Pavlov 2002 for a review). Thermal radiation from a few NSs was also detected in the optical-UV energy range with the *Hubble Space Telescope* (e. g., Pavlov, Stringfellow & Córdoba 1996; Walter & Matthews 1997). Currently operating X-ray observatories, *Chandra* and *XMM-Newton*, are providing new excellent data on X-rays from NSs (see the contributions by Weisskopf, Becker, and Pavlov, Zavlin & Sanwal in these Proceedings).

To interpret these observations, one needs reliable models for the NS thermal radiation. The fact that the spectrum of radiation emergent from a NS atmosphere can be very different from a blackbody spectrum, and the angular distribution can be very far from isotropic, particular in a strong magnetic field, has been recognized long ago. For instance, Pavlov & Shibano (1978) calculated spectra and angular distributions of radiation from a strongly magnetized NS atmosphere assuming the source function grows inward linearly in the emitting layers. First self-consistent models for NS atmospheres were developed by Romani (1987), for low magnetic fields, and Shibano et al. (1992), for strong magnetic fields. Since then, various aspects of the NS atmosphere modeling have been investigated in many papers. Below we will overview the current status of this field and summarize some important results.

2. Distinctive features of NS atmospheres

The NS thermal radiation emerges, as in usual stars, in superficial layers which can be in a gaseous state (atmosphere) or a condensed state (liquid or solid surface), depending on surface temperature, magnetic field and chemical composition. A condensed surface forms at low temperatures and very strong magnetic fields. For instance, according to the estimates by Lai & Salpeter (1997), hydrogen is condensed in surface layers if $T \lesssim 1 \times 10^5$ K at $B = 1 \times 10^{13}$ G ($T \lesssim 1 \times 10^6$ K at $B = 5 \times 10^{14}$ G). At higher temperatures and/or lower magnetic fields, hydrogen does not condensate and forms an atmosphere.

In both usual stars and NSs the properties of radiation emergent from an atmosphere strongly depend on

its chemical composition. The difference between usual stars and NSs is that in NSs we expect the emitting layers to be comprised of just one, lightest available, chemical element, not a mixture of elements, because heavier elements sink into deeper layers due to the immense NS gravitation (Alcock & Illarionov 1980). For instance, even a small amount of hydrogen (with a surface density of $\sim 1 \text{ g cm}^{-2}$) is sufficient for the radiation to be indistinguishable from that emitted from a purely hydrogen atmosphere. Such an amount of hydrogen, $\gtrsim 10^{-20} M_{\odot}$, can be delivered onto the NS surface by, e. g., accretion from the interstellar medium and/or fallback of a fraction of the envelope ejected during the supernova explosion. If no hydrogen is present at the surface, a heavier chemical element is responsible for the radiative properties of the NS atmosphere. However, a mixture of elements can be observed in the emitting layers if the NS is experiencing accretion with such a rate that the accreting matter is supplied faster than the gravitational separation occurs. Therefore, it is important to construct the NS atmosphere models for a variety of surface compositions, both ‘pure’ and mixed.

The gravitational separation of elements is one of the consequences of the enormous gravity at the NS surface, with the gravitational acceleration $g \sim 10^{14} - 10^{15} \text{ cm s}^{-2}$. The gravity makes NS atmospheres very thin, $\sim 0.1 - 10 \text{ cm}$, and dense, $\rho \sim 10^{-2} - 10^2 \text{ g cm}^{-3}$. Such a high density causes strong nonideality effects (pressure ionization, smoothed spectral features) which must be taken into account (e. g., Pavlov et al. 1995). In addition, the strong gravitational field bends the photon trajectories near the NS surface (Pechenick, Ftaclas & Cohen 1983), as illustrated by the sketch in Figure 1. This effect depends on the gravitational parameter $g_r = (1 - 2GM/c^2R)^{1/2}$, and it can even make the whole NS surface visible if the NS is massive enough, $M > 1.8 (10 \text{ km}/R) M_{\odot}$. In particular, the gravitational bending strongly affects the observed pulsations of thermal emission (Zavlin, Shibano & Pavlov 1995a).

Huge magnetic fields, $B \sim 10^{11} - 10^{14} \text{ G}$, in the surface layers of many NSs change the properties of the atmospheric matter and the emergent radiation even more drastically. Strongly magnetized NS atmospheres are essentially anisotropic, with radiative opacities depending on the magnetic field and the direction and polarization of radiation. Moreover, since the ratio of the cyclotron energy, $E_{ce} = \hbar eB/m_e c$, to the Coulomb energy is very large (e.g., $\gamma \equiv E_{ce}/(1 \text{ Ry}) = 850 (B/10^{12} \text{ G})$ for a hydrogen atom), the structure of atoms is strongly distorted by the magnetic field. For instance, the binding (ionization) energies of atoms are increased by a factor of $\sim \ln^2 \gamma$ (e. g., the ionization potential of a hydrogen atom is about 310 eV at $B = 10^{13} \text{ G}$). This, in turn, significantly modifies ionization equilibrium of the NS atmospheric matter. Another important effect is that the heat conductivity of the NS crust is anisotropic (it is higher along the magnetic

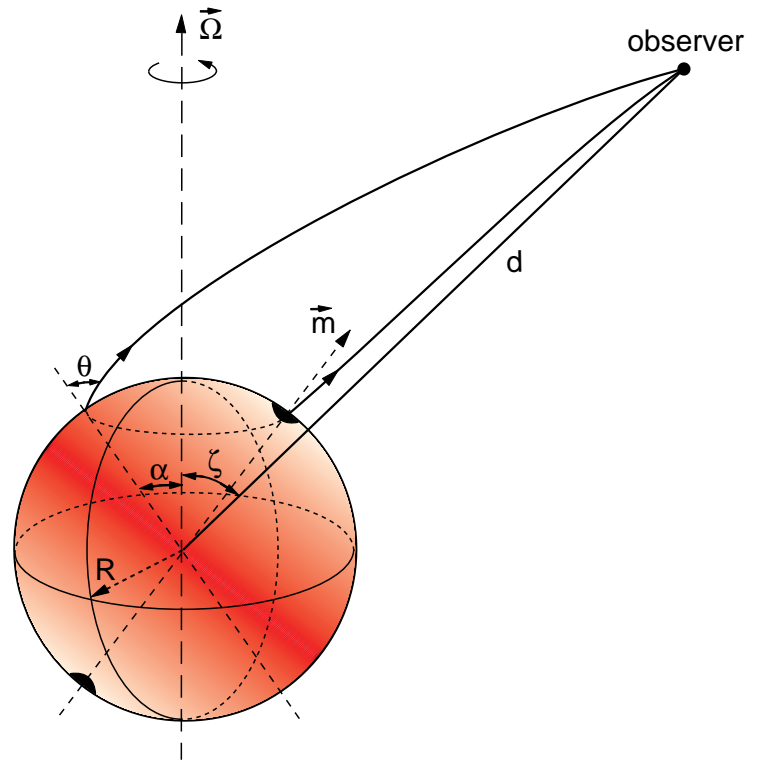


Fig. 1. Bending of photon trajectories in a strong gravitational field near the surface of a NS with rotational and magnetic axes Ω and m , respectively.

field). This results in a nonuniform surface temperature distribution (Greenstein & Hartke 1983), which leads to pulsations of the thermal radiation due to NS rotation.

3. Atmosphere models with low magnetic fields

Some NSs (e.g., millisecond pulsars) have relatively low magnetic fields, $B \lesssim 10^9 \text{ G}$. In such magnetic fields the electron cyclotron energy, $E_{ce} \lesssim 0.01 \text{ keV}$, is lower than the binding energy of atoms and thermal energy of particles. As a result, the effect of the field on the radiative opacities and emitted spectra is negligible, at X-ray energies, $E \gtrsim 0.1 \text{ keV}$. Hence, to model low-field NS atmospheres, one can merely put $B = 0$. These models are applicable to millisecond pulsars, NS transients in quiescence (e.g., Rutledge et al. 2002), and, perhaps, to some radio-quiet isolated NSs. One should remember, however, that the magnetic field effects on spectral opacity at optical wavelengths must be included even for these low fields if the models are applied for interpreting the optical spectra.

First models of low-field NS atmospheres were presented in the pioneering work by Romani (1987). Since

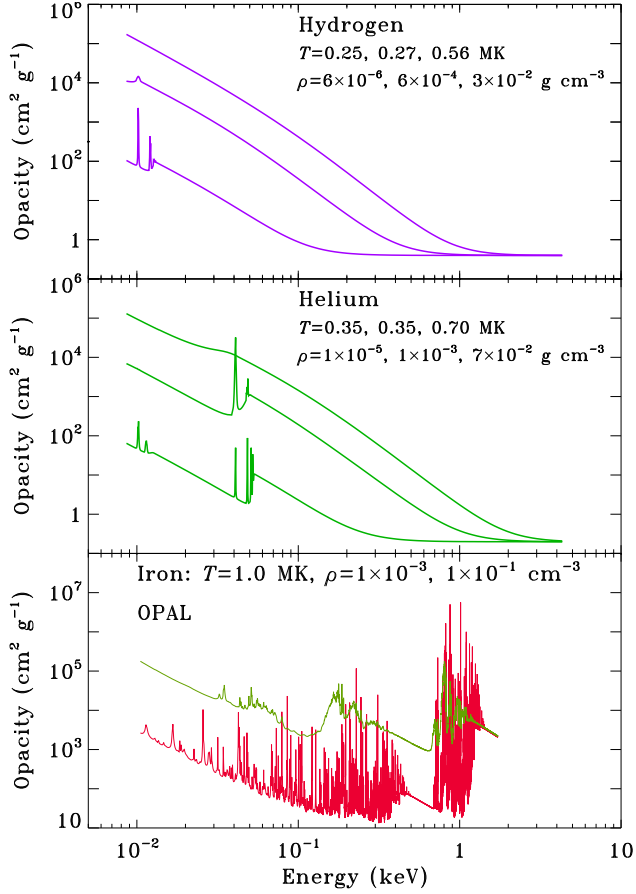


Fig. 2. Radiative spectral opacity k_ν for hydrogen, helium and iron plasmas at different temperatures and densities (magnetic field $B = 0$). The iron opacity is provided by the OPAL group (Rogers & Iglesias 1994).

then, models for various surface chemical compositions have been developed by Rajagopal & Romani (1996), Zavlin, Pavlov & Shibano (1996), Pavlov & Zavlin (2000a), Werner & Deetjen (2000), Pons et al. (2002), Gänsicke, Braje & Romani (2002).

3.1. General approach

As the thickness of a NS atmosphere is much smaller than the NS radius, $R \approx 10$ km, NS atmospheres can be considered in the plane-parallel approximation. In addition, rather high densities of the surface layers allow one to consider the atmospheres to be in local thermodynamic equilibrium.

The standard approach for the atmosphere modeling includes solving of three main equations. The first one is the radiative transfer equation for the specific spectral intensity I_ν (e. g., Mihalas 1978):

$$\mu \frac{d}{dy} I_\nu = k_\nu (I_\nu - S_\nu), \quad (1)$$

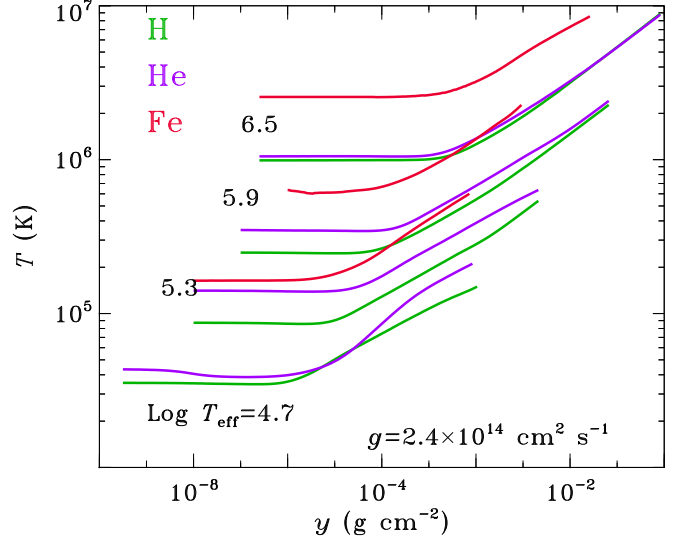


Fig. 3. Temperature dependences $T(y)$ in nonmagnetic atmosphere models with different effective temperatures and chemical compositions.

where μ is cosine of the angle θ between the normal to the atmosphere and the wave-vector of radiation, y is the column density ($dy = \rho dz$, with z being the geometrical depth), $k_\nu = \alpha_\nu + \sigma_\nu$ is the total radiative opacity which includes the ‘true absorption’ (α_ν) and scattering (σ_ν) opacities, $S_\nu = (\sigma_\nu J_\nu + \alpha_\nu B_\nu) k_\nu^{-1}$ is the source function, $J_\nu = \frac{1}{2} \int_{-1}^1 I_\nu d\mu$ is the mean spectral intensity, and B_ν is the Planck function. The boundary condition for this equation is $I_\nu = 0$ for $\mu < 0$ at $y = 0$, assuming no incident radiation at the NS surface.

NS atmospheres are usually considered to be in radiative and hydrostatic equilibrium. The first condition implies that the total energy flux through the atmosphere is constant and transferred solely by radiation,

$$\int_0^\infty d\nu \int_{-1}^1 \mu I_\nu d\mu = \sigma_{\text{SB}} T_{\text{eff}}^4, \quad (2)$$

where T_{eff} is the effective temperature, and σ_{SB} is the Stefan-Boltzmann constant. The second condition means that the atmospheric pressure is $P = gy$ (the radiative force is insignificant unless $T_{\text{eff}} \gtrsim 10^7$ K). Finally, these three equations are supplemented with the equation of state for the atmospheric plasma and equations of ionization equilibrium. The latter is needed for computing the electron number density and the fractions of ions in different stages of ionization to obtain the radiative opacity with account for free-free, bound-free and bound-bound transitions (see examples in Fig. 2)¹. A detailed descrip-

¹ Opacities of heavy chemical elements used in this work were calculated by the OPAL group:

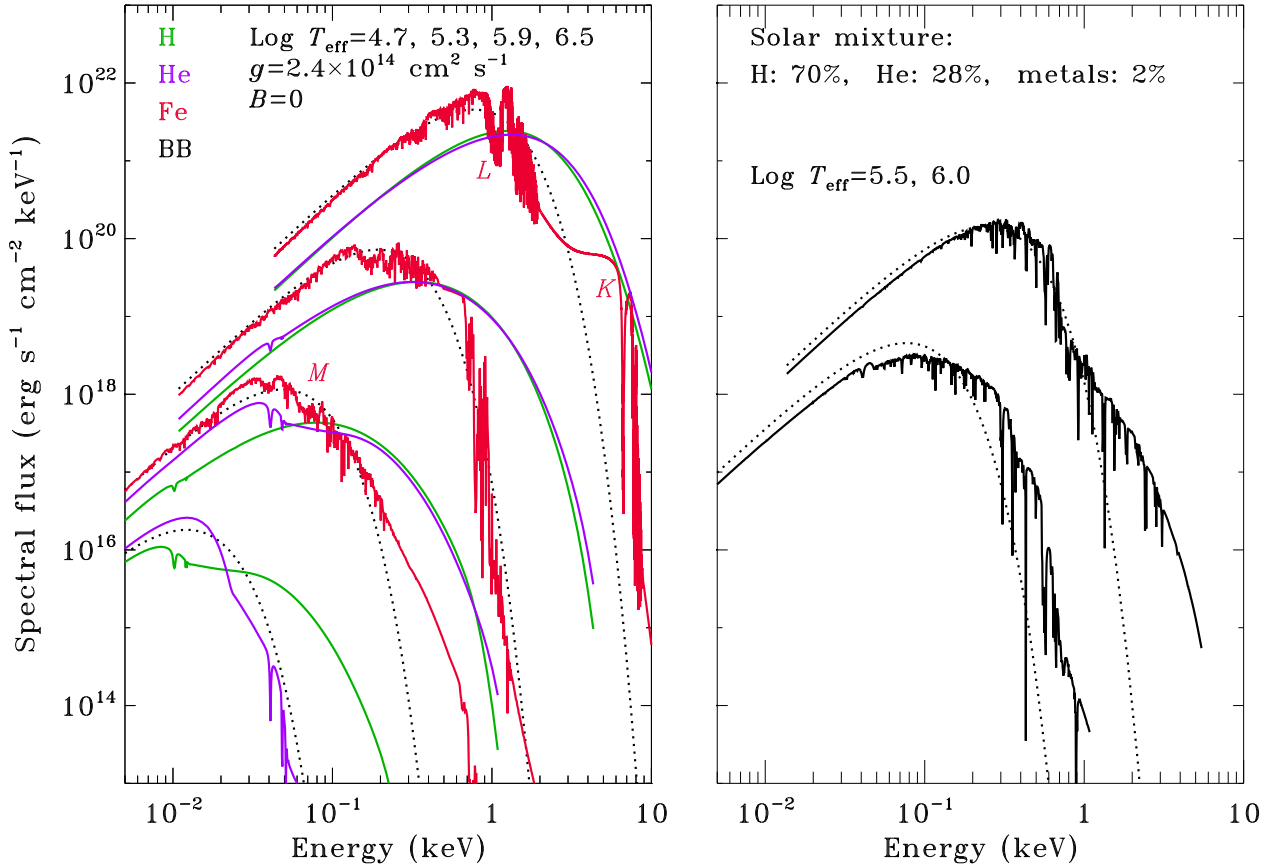


Fig. 4. Spectral fluxes of emergent radiation in nonmagnetic atmosphere models for several effective temperatures and chemical compositions.

tion of the model computations can be found, e.g., in Zavlin et al. (1996).

3.2. Results

To explain the main properties of the atmosphere emission, we first present in Figure 3 the most important property of the atmospheric structure responsible for the emergent radiation — the depth dependence of the temperature in the NS surface layers, $T(y)$.

Figure 4 presents the spectral fluxes of emergent radiation at a local surface point, $F_\nu = \int_0^1 \mu I_\nu d\mu$ (at $y = 0$), for several effective temperatures and chemical compositions (pure hydrogen, helium and iron, and a solar mixture), together with the blackbody spectral fluxes at the same T_{eff} . The model spectra differ substantially from the blackbody spectra, particularly in high-energy tails of the spectra of light-element (hydrogen and helium) atmospheres². The reason for such behavior is in the rapid decrease of the light-element opacities with energy ($\sim E^{-3}$, see the upper and middle panels in Fig. 2), so that the high-energy radi-

ation is formed in deeper and hotter layers (Fig. 3). Since the radiative opacity is large at lower energies, the low-energy photons escape from very superficial layers with a temperature $T(0) < T_{\text{eff}}$. Therefore, the low-energy tails of the model spectra are suppressed with respect to the Rayleigh-Jeans spectra at the same T_{eff} .

The spectra emitted from the heavy-element atmospheres (iron and solar mixture) exhibit numerous spectral lines and photoionization edges (e. g., M, L and K spectral complexes in the iron spectra) produced by ions in various ionization stages. Generally, they are closer to the blackbody radiation because the energy dependence of the heavy-element opacities is, on average, flatter than that for the light elements (see examples in the bottom panel of Fig. 2). However, local deviations from the blackbody spectra can be very substantial. Moreover, the spectral features can be rather strong even if metals contribute as little as 0.05% of the total NS atmosphere composition (see Fig. 5).

Although the opacity of the atmospheric plasma is isotropic in the nonmagnetic case, the emitted radiation show substantial anisotropy, i. e., the specific intensity I_ν depends on the direction of emission due to the limb-

² The nonmagnetic hydrogen atmosphere models are available at <http://legacy.gsfc.nasa.gov/docs/xanadu/xspec>

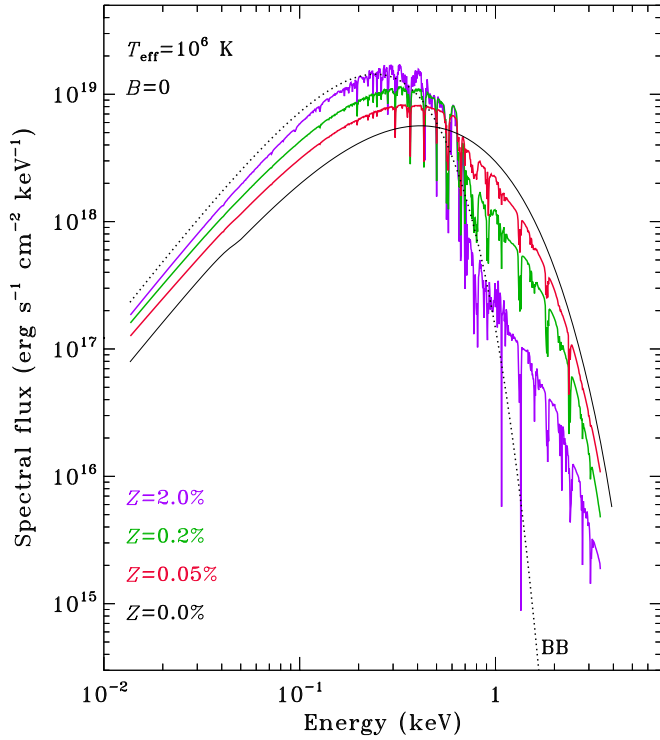


Fig. 5. Spectral fluxes of emergent radiation in nonmagnetic models with different metal abundances Z ($Z = 2.0\%$ corresponds to the standard solar mixture of elements — see Grevesse & Noels 1993).

darkening effect (Fig. 6). At large values of the angle θ between the normal to the surface and the wave-vector the emerging photons are produced in shallow layers with lower temperatures. The anisotropy depends on photon energy and chemical composition of the atmosphere. This effect should be taken into account to model thermal radiation from a nonuniform NS surface (see Section 5).

The emergent radiation depends also on the surface gravity: a stronger gravitational acceleration increases the density of the atmospheric plasma and enhances the non-ideality effects, which results in weaker (more smoothed) spectral features (see examples in Fig. 6 of Zavlin et al. 1996). However, this effect is rather small and might be important only for analyzing observational data of extremely good statistics.

4. Atmosphere models with strong magnetic fields

It is commonly believed that most NSs (at least active radio/X-ray/ γ -ray pulsars) have rather strong surface magnetic fields, $B \sim 10^{10}$ – 10^{14} G. Such fields drastically change the properties of NS atmospheres, as discussed above. Magnetic hydrogen models have been developed by Shibano et al. (1992), Pavlov et al. (1994), Shibano & Zavlin (1995), Pavlov et al. (1995), and Zavlin et al. (1995b). These models use simplified radiative

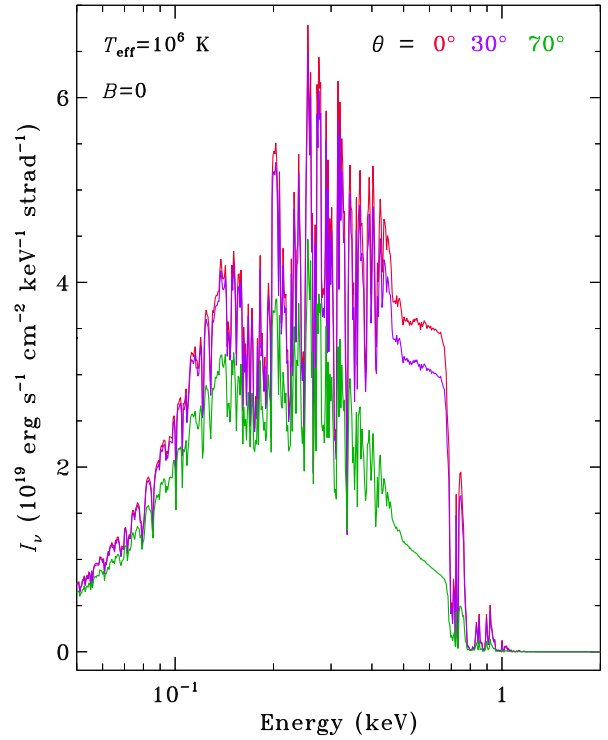


Fig. 6. Spectra of specific intensities I_ν emitted from an iron atmosphere with $T_{\text{eff}} = 1 \times 10^6$ K, at different angles θ ($\mu = \cos\theta$).

opacities of strongly magnetized, partially ionized plasma, which do not include the bound-bound transitions. However, they are considered to be reliable enough in the case of high temperatures ($T_{\text{eff}} \gtrsim 10^6$ K at typical radio-pulsar fields $\sim 10^{12}$ G), when the atmospheric plasma is almost fully ionized even in the strong magnetic fields. Recently, completely ionized hydrogen models for superstrong magnetic fields, $B \sim 10^{14}$ – 10^{15} G, have been presented in a number of papers (Bezchastnov et al. 1996; Bulik & Miller 1997; Özel 2001; Ho & Lai 2001; Zane et al. 2001), concerned mainly with the vacuum polarization effects (Pavlov & Gnedin 1984) and the ion cyclotron lines whose energies get into the X-ray band at $B \gtrsim 2 \times 10^{13}$ G. A set of magnetic iron models was constructed by Rajagopal, Romani & Miller (1997), with the use of rather crude approximations for the very complicated properties of iron ions in strong magnetic fields. The iron atmosphere spectra show many prominent spectral features which could be very useful to measure the NS magnetic field and the mass-to-radius ratio.

4.1. General approach

Modeling magnetic NS atmospheres is generally similar to the nonmagnetic case. The main difference is that the atmospheric radiation is polarized, and the radiative opacities depend on the polarization and direction of radiation.

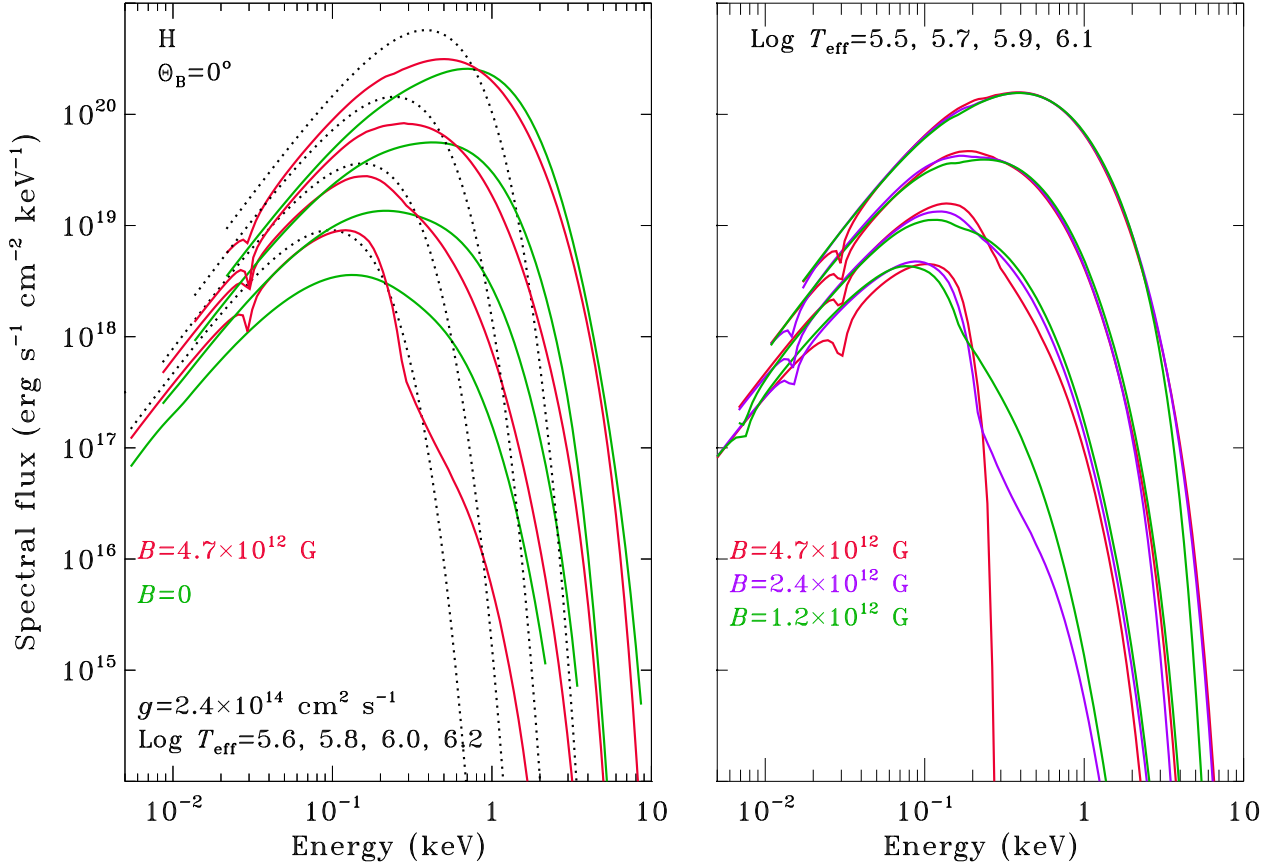


Fig. 7. Spectral fluxes of radiation emerging from magnetic hydrogen atmospheres, for several effective temperatures and magnetic fields perpendicular to the surface.

Gnedin & Pavlov (1974) described the radiative transfer in a strongly magnetized plasma in terms of coupled equations for specific intensities of two normal modes, $I_{\nu,1}$ and $I_{\nu,2}$, with different polarizations and opacities:

$$\mu \frac{d}{dy} I_{\nu,j}(\mathbf{n}) = k_{\nu,j}(\mathbf{n}) I_{\nu,j}(\mathbf{n}) - \left[\sum_{i=1}^2 \oint d\mathbf{n}' I_{\nu,i}(\mathbf{n}') \sigma_{\nu,ij}(\mathbf{n}', \mathbf{n}) + \alpha_{\nu,j}(\mathbf{n}) \frac{B_{\nu}}{2} \right], \quad (3)$$

where \mathbf{n} is the (unit) wave-vector, $\alpha_{\nu,j}$ is the absorption opacity for the j -th mode, and $\sigma_{\nu,ij}$ is the scattering opacity from mode i to mode j . It should be noted that the opacity depends on the angle between the wave-vector and the magnetic field, so that I_{ν} depends not only on θ , but also on Θ_B , the angle between the local magnetic field and the normal to the NS surface. Similar to the nonmagnetic case, equations (3) are supplemented with the equations of radiative and hydrostatic equilibrium. To overcome the problems with the sharp angular dependence of the radiative opacities (Kaminker, Pavlov & Shibano 1982), a two-step method for modeling of magnetic NS atmospheres was developed (Pavlov et al. 1994; Shibano &

Zavlin 1995). At the first step, the radiative transfer is solved in the diffusion approximation for the mean intensities $J_{\nu,j} = (4\pi)^{-1} \oint I_{\nu,j}(\mathbf{n}) d\mathbf{n}$:

$$\frac{d}{dy} d_{\nu,j} \frac{d}{dy} J_{\nu,j} = \bar{\alpha}_{\nu,j} \left[J_{\nu,j} - \frac{B_{\nu}}{2} \right] + \bar{\sigma}_{\nu} [J_{\nu,j} - J_{\nu,3-j}], \quad (4)$$

where $d_{\nu,j}$ is the diffusion coefficient, $\bar{\alpha}_{\nu,j}$ and $\bar{\sigma}_{\nu}$ are the angle-averaged absorption and scattering opacities (see Pavlov et al. 1995 for details). Next, the atmospheric structure obtained at the first step is corrected using an iterative procedure applied to the exact equations of the radiative transfer.

4.2. Results

Figure 7 shows polarization-summed spectral fluxes of the emergent radiation, $F_{\nu} = \int_0^1 \mu (I_{\nu,1} + I_{\nu,2}) d\mu$, emitted by a local element of the NS surface, for several values of effective temperature and magnetic field perpendicular to the surface ($\Theta_B = 0$). The main result is that the magnetic model spectra are harder than the blackbody radiation of the same T_{eff} , although they are softer than the low-field spectra. Similar to the low-field case, this is explained by

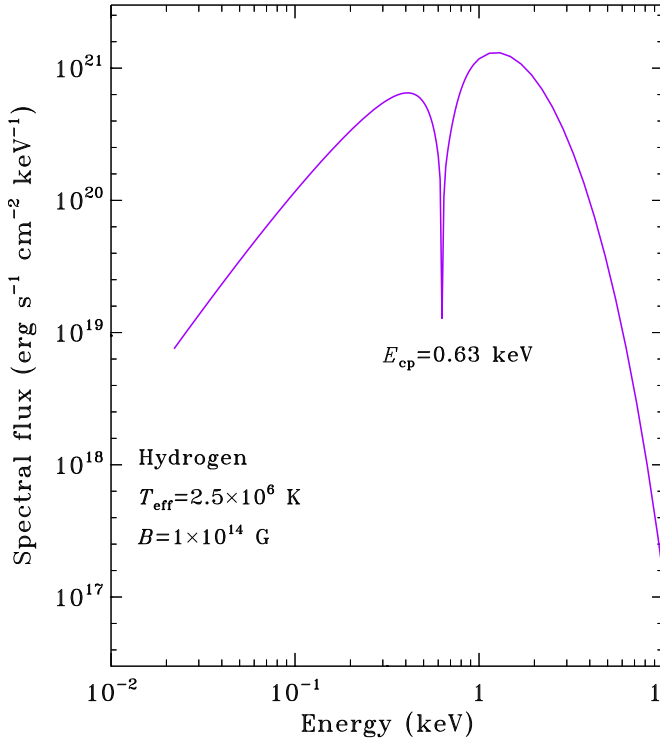


Fig. 8. Spectral flux of radiation emerging from an atmosphere with $B = 10^{14}$ G, with a strong proton cyclotron line.

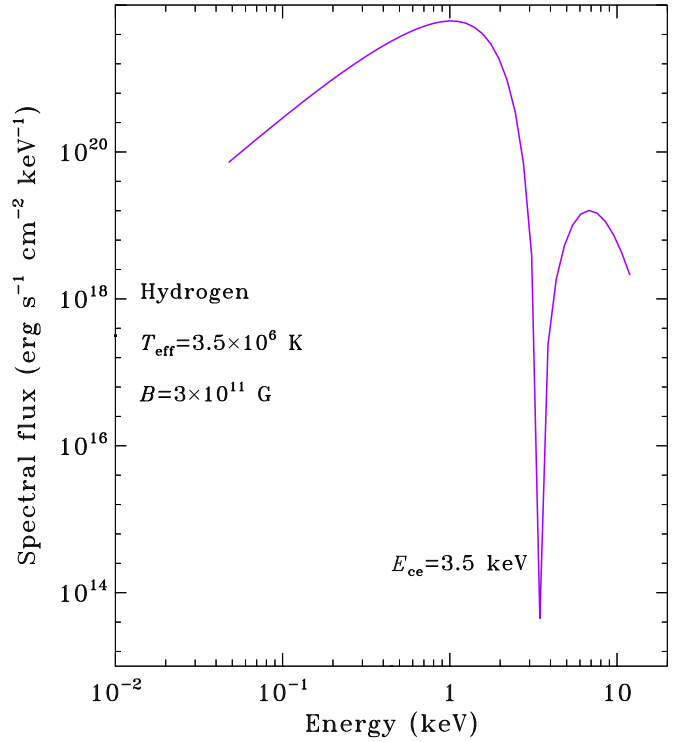


Fig. 9. Spectral flux of radiation emerging from an atmosphere with $B = 3 \times 10^{11}$ G, with a strong electron cyclotron line.

the temperature growth with depth and the opacity decrease at higher energies, which is more gradual ($\propto E^{-1}$ for the mode with smaller opacity) compared to the non-magnetic case. At lower effective temperatures, $T_{\text{eff}} \lesssim 10^6$ K, the photoionization opacity is important, and the dependence of the spectra on magnetic field becomes more pronounced (see the right panel in Fig. 7). The field dependence is most clearly seen, at T_{eff} sufficiently high to provide strong ionization, in the proton cyclotron lines centered at energies $E_{\text{cp}} = 6.3 (B/10^{12} \text{ G})$ eV. If the magnetic field is very large, $B \gtrsim 10^{14}$ G, the proton cyclotron line shifts into the X-ray band and can be very strong (see Fig. 8). On the other hand, if the magnetic field is not so large, $B = 10^{10}$ – 10^{12} G, the NS atmosphere spectra may exhibit the electron cyclotron lines in the X-ray band, at $E_{\text{ce}} = 11.6 (B/10^{12} \text{ G})$ keV (see Fig. 9).

First calculations of hydrogen atmosphere models which include bound-bound transitions show that spectral lines, considerably broadened by the motional Stark effect (Pavlov & Mészáros 1993; Pavlov & Potekhin 1995) become prominent at $T_{\text{eff}} \lesssim 5 \times 10^5$ K. The strongest line corresponds to the transition between the ground state and the lowest excited state; its energy is $E \approx [75(1 + 0.13 \ln(B/10^{13} \text{ G}) + 63(B/10^{13} \text{ G}))]$ eV, at $B \sim 10^{13}$ G (see examples in Fig. 10).

Radiation emerging from a magnetized NS atmosphere is strongly anisotropic. Angular dependences of the lo-

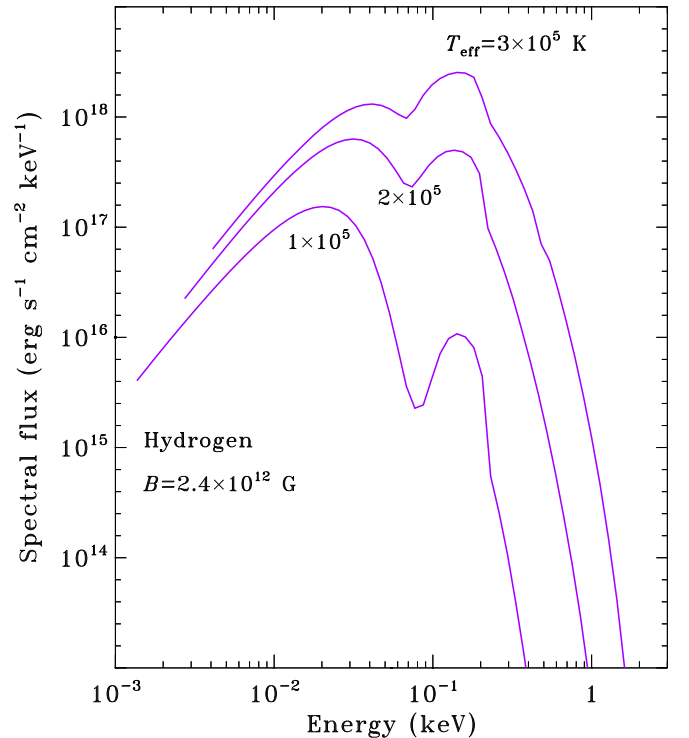


Fig. 10. Spectral fluxes of radiation emerging from hydrogen atmospheres with $B = 2.4 \times 10^{12}$ G and different values of T_{eff} , with bound-bound transitions included.

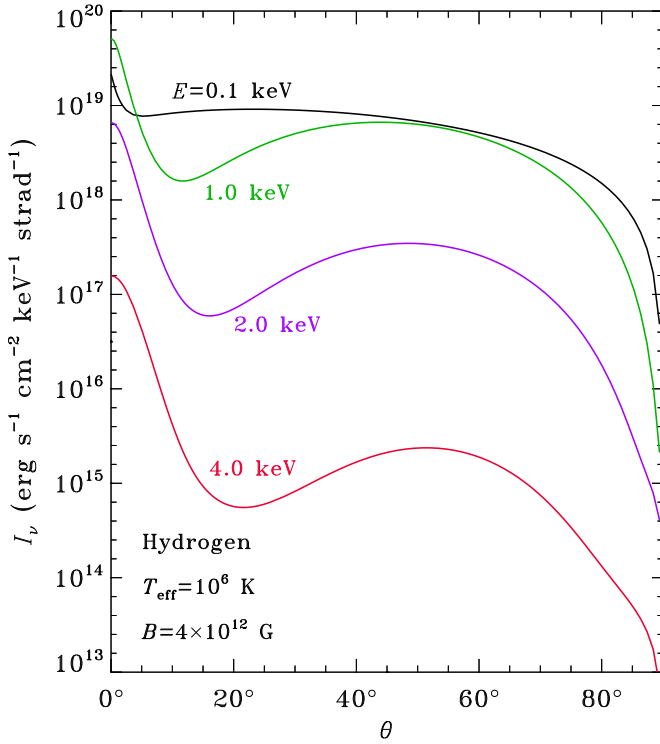


Fig. 11. Angular dependences of polarization-summed specific intensities at different photon energies E in the hydrogen atmosphere model with $T_{\text{eff}} = 1 \times 10^6$ K and magnetic field $B = 4 \times 10^{12}$ G, perpendicular to the surface.

cal specific intensities, $I_\nu = I_{\nu,1} + I_{\nu,2}$, show a complicated “pencil-plus-fan” structure — a narrow peak along the direction of the magnetic field (where the atmospheric plasma is most transparent for the radiation), and a broader peak at intermediate angles. The widths and strengths of the peaks depend on magnetic field and photon energy (see examples in Fig. 11). Obviously, it is very important to account for this anisotropy while modeling the radiation from a NS with nonuniform surface magnetic field, effective temperature, and chemical composition.

5. Thermal radiation as seen by a distant observer

Results presented in Sections 3 and 4 describe spectral radiation emitted by a *local* element at the NS surface. The effective temperature and/or magnetic field distributions over the NS surface can be nonuniform (for example, if a NS has a dipole magnetic field, the effective temperature decreases from the magnetic poles to the equator). To calculate the *total* NS emission, one has to integrate the local intensities, computed for local temperatures and magnetic fields, over the visible part of the NS surface S ,

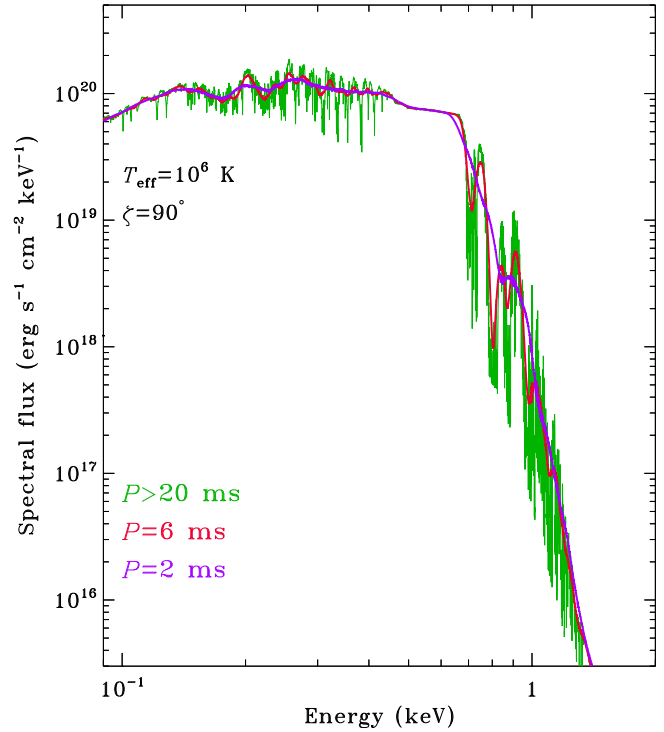


Fig. 12. Spectral fluxes of radiation from the *whole* surface of a nonmagnetic NS covered with an iron atmosphere at $T_{\text{eff}} = 1 \times 10^6$ K. The (unredshifted) spectra are calculated for different NS rotation periods P , at the inclination of rotational axis $\zeta = 90^\circ$.

with account for the gravitational redshift and bending of photon trajectories:

$$F(E) = g_r \frac{1}{D^2} \int_S \mu I(E/g_r) dS, \quad (5)$$

where D is the distance from the NS to the observer, and E is the *observed* (redshifted) energy³. More details about the integration over the NS surface can be found in Pavlov & Zavlin (2000b). It should be noted that if a NS has a nonuniform (e.g., dipole) distribution of the magnetic field, the integration broadens the spectral features (in particular, cyclotron resonance lines — see Zavlin et al. 1995b; Pavlov & Zavlin 2000b; Zane et al. 2001).

If the NS is a fast rotator, one should take into account the Doppler shifts of energies of photons emitted from surface elements moving with different radial velocities. Maximum values of these velocities, $v_r = 2\pi R P^{-1} \sin \zeta$ (P is the rotation period, ζ the inclination of the rotation axis), can be as high as 10%–15% of the speed of light for millisecond periods. Figure 12 presents (unredshifted) spectra emitted from the whole NS surface covered with

³ To take into account the interstellar absorption, a factor of $\exp[-n_{\text{H}}\sigma_{\text{eff}}(E)]$ should be added in eq. (5) [$\sigma_{\text{eff}}(E)$ is the absorption cross section per hydrogen atom].

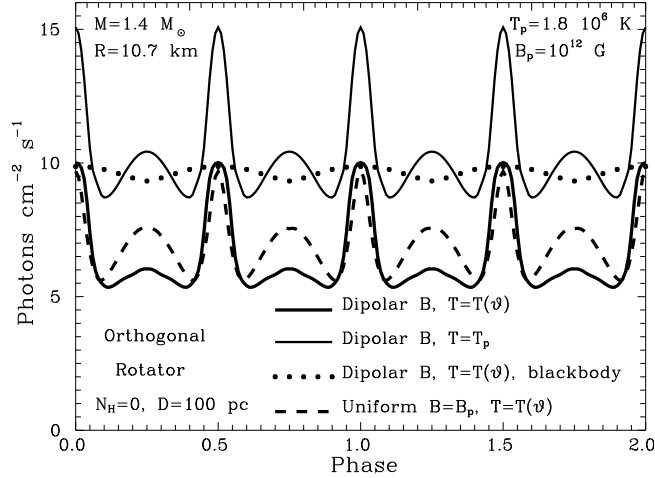


Fig. 13. Energy-integrated light curves of a rotating NS with different distributions of surface temperature and magnetic field (from Shibano et al. 1995). The temperature is either uniform, $T = T_p$, or nonuniform, $T = T(\vartheta)$, as given by computations with account for the anisotropy of the heat conductivity in the NS crust (ϑ is magnetic colatitude, T_p and B_p are the effective temperature and the field at the magnetic poles). The NS rotational axis is perpendicular to both the magnetic axis and the line of sight ($\alpha = \zeta = 90^\circ$).

an iron atmosphere (nonmagnetic case). For slowly rotating NSs, $P \gtrsim 20$ ms, there is no significant effect on the emergent radiation. Fast rotation, $P \lesssim 10$ ms, may lead to complete smearing of weak and narrow spectral lines, provided $\sin \zeta$ is large enough, leaving only most prominent spectral jumps around the strongest photoionization edges.

In the case of radio pulsars, a fraction of the observed thermal X-ray radiation is emitted from small hot spots (polar caps) around the NS magnetic poles. These polar caps can be heated up to X-ray temperatures by relativistic particles impinging on the poles from the acceleration zone in the pulsars' magnetosphere. In the case of millisecond pulsars, with characteristic ages of 10^8 – 10^9 yr, the whole NS surface (except for the polar caps) is believed to be too cold ($T_{\text{eff}} \lesssim 10^5$ K) to be observable in X-rays, so the detected thermal emission can be modeled as emitted from small heated spots:

$$F(E) = g_r \frac{S_a}{D^2} I(E/g_r, \theta^*), \quad (6)$$

where the apparent spot area S_a and the angle θ^* between the wave-vector and the radius-vector to the hot spot are computed with account for the effect of gravitational bending. These quantities depend on the angles α (between the rotational and magnetic axes) and ζ (between the rotational axis and the line of sight — see Fig. 1), and the gravitational parameter g_r (see Zavlin et al. 1995a for details).

The flux given by equations (5) or (6) varies with the period of NS rotation. One can obtain a large variety of pulse profiles at different assumptions on the angles α and

ζ and the NS mass-to-radius ratio. Examples of pulse profiles computed for radiation from the whole NS surface are shown in Figure 13; pulse profiles of thermal radiation from heated polar caps are presented by Zavlin et al. (1995a).

Although the model atmosphere spectra are different from the blackbody spectra, very often an observed thermal spectrum can be fitted equally well with the blackbody and NS atmosphere models, particularly when the energy resolution is low and/or the energy band is narrow. However, the parameters obtained from such fits are quite different, especially when the hydrogen or helium atmospheres are used. Since the light-element atmosphere spectra are much harder than the blackbody spectra at the same effective temperature, atmosphere model fits give temperatures T_{atm} significantly lower than the blackbody temperature T_{bb} , with a typical ratio $T_{\text{bb}}/T_{\text{atm}} \sim 2$ – 3 (see, for example, Pavlov et al. 1996; Pons et al. 2002). On the other hand, to provide the same total energy flux, the blackbody fit gives a smaller normalization factor, proportional to S/D^2 , than the atmosphere model fit. In other words, the light-element atmosphere fit gives a considerably larger size of the emitting region, $S_{\text{atm}}/S_{\text{bb}} \sim 50$ – 200 , for the same distance to the source.

6. Conclusions

In the recent decade, substantial progress has been made in modeling atmospheres of isolated NSs. Best investigated cases are nonmagnetic atmospheres and fully-ionized light-element atmospheres with strong magnetic fields. The atmosphere models have been applied to the

interpretation of thermal emission from NSs of different types. For instance, Pavlov & Zavlin (1997), Zavlin & Pavlov (1998), and Zavlin et al. (2002) analyzed the X-ray emission from the millisecond pulsar J0437–4715 using the nonmagnetic light-element atmosphere models; Pavlov et al. (2001) applied the magnetic hydrogen models to the analysis of radiation from the Vela pulsar; Zavlin, Pavlov & Trümper (1998) and Zavlin, Trümper & Pavlov (1999) used the magnetic light-element models to interpret the thermal emission from NSs in the supernova remnants PKS 1209–51/52 and Puppis A. More examples are presented in the contribution by Pavlov et al. in this volume.

However, a number of problems in the atmosphere modeling remains to be solved. First of all, investigations of the structure of various atoms, molecules, and molecular chains in strong magnetic fields, as well as radiative transitions in these species (Pavlov 1998), are necessary to construct magnetic atmosphere models of different chemical compositions. First efforts in this direction are being undertaken (Mori & Hailey 2002). Particularly interesting are the (virtually unknown) radiative properties of matter in superstrong magnetic fields, $B \gtrsim 10^{14}$ G, apparently found in anomalous X-ray pulsars and soft gamma-ray repeaters. Further work is needed on radiative properties of nonideal plasmas and condensed matter. These investigations will eventually result in more advanced models for thermal radiation of isolated NS, needed for the interpretation of high-quality observations of these objects with the *Chandra* and *XMM-Newton* X-ray observatories.

Acknowledgements. The authors gratefully acknowledge the support by the Heraeus foundation and the hospitality of the Physikzentrum Bad Honnef. Work of GGP was partially supported by NASA grant NAG5-10865.

References

- Alcock C., Illarionov A.F., 1980, *ApJ*, 235, 534
 Becker W., Pavlov G.G., 2002, in *The Century of Space Science*, eds. J. Bleeker, J. Geiss & M. Huber (Dordrecht: Kluwer), in press
 Bezchastnov V.G., Pavlov G.G., Shibano Yu.A., Zavlin V.E., 1996, in *Gamma-ray Bursts*, Proc. 3rd Huntsville Symp., AIP Conf. Proc., v.384, eds. C. Kouveliotou, M. Briggs & G.J. Fishman (NY: Woodbury), p.907
 Bulik T., Miller M.C., 1997, *MNRAS*, 288, 596
 Brinkmann W., Ögelman H., 1987, *A&A*, 182, 71
 Cheng A.F., Helfand D.J., 1983, *ApJ*, 271, 271
 Chiu H.Y., Salpeter E.E., 1964, *Phys. Rev. Lett.*, 12, 413
 Córdova F.A., Hjellming R.M., Mason K.O., Middleditch J., 1989, *ApJ*, 345, 451
 Gänsicke B.T., Braje T.M., Romani R.W., 2002, *A&A*, 386, 1001
 Gnedin Yu.N., Pavlov G.G., 1974, *Sov. Phys.-JETP*, 38, 903
 Greenstein G., Hartke G.J., 1983, *ApJ*, 271, 283
 Grevesse N., Noels A., 1993 in *Origin and Evolution of the Elements*, eds. E. Prantzos, M. Vaugioni-Flam & M. Gasse (Cambridge University Press), p.14
 Ho W.C.G., Lai D., 2001, *MNRAS*, 327, 1081
 Kaminker A.D., Pavlov G.G., Shibano Yu.A., 1982, *Ap&SS*, 86, 249
 Kellet B.J., et al., 1987, *MNRAS*, 225, 199
 Lai D., Salpeter E.E., 1997, *ApJ*, 491, 270
 Mihalas D., 1978, *Stellar Atmospheres* (San Francisco: Freeman)
 Mori, K., Hailey, C.J. 2002, *ApJ*, 564, 914
 Özel F., 2001, *ApJ*, 563, 276
 Pavlov G.G., 1998, in *Atoms and Molecules in Strong External Fields*, eds. P. Schmelcher & W. Schweizer (New York: Plenum), p.37
 Pavlov G.G., Shibano Yu.A., 1978, *Sov. Astron.*, 22, 214
 Pavlov G.G., Gnedin Yu.N., 1984, *Astrophys. Space Phys. Rev.*, 3, 197
 Pavlov G.G., Mészáros P., 1993, *ApJ*, 416, 752
 Pavlov G.G., Potekhin Y.A., 1995, *ApJ*, 450, 883
 Pavlov G.G., Zavlin V.E., 1997, *ApJ*, 490, L91
 Pavlov G.G., Zavlin V.E. 2000a, in *Highly Energetic Physical Processes and Mechanisms for Emission from Astrophysical Plasmas*, IAU Symp. 195, eds. P.C.H. Martens, S. Tsuruta & M.A. Weber (PASP), p.103
 Pavlov G.G., Zavlin V.E., 2000b, *ApJ*, 529, 1011
 Pavlov G.G., Shibano Yu.A., Ventura J., Zavlin V.E., 1994, *A&A*, 289, 847
 Pavlov G.G., Shibano Yu.A., Zavlin V.E., Meyer R.D., 1995, in *The Lives of Neutron Stars*, eds. A. Alpar, U. Kilizóglu & J. van Paradijs (Dordrecht: Kluwer), p.71
 Pavlov G.G., Stringfellow G.S., Córdova F.A., 1996, *ApJ*, 489, L75
 Pavlov G.G., Zavlin V.E., Trümper J., Neuhäuser R., 1996, *ApJ*, 472, L33
 Pavlov G.G., Zavlin V.E., Sanwal D., Burwitz V., Garmire G.P., 2001, *ApJ*, 552, L129
 Pechenick K.R., Ftaclas C., Cohen J.M., 1983, *ApJ*, 274, 846
 Pons J.A., Walter F.M., Lattimer J.M., Prakash M., Neuhäuser R., An P., 2002, *ApJ*, 564, 981
 Rajagopal M., Romani R.W. 1996, *ApJ*, 461, 327
 Rajagopal M., Romani R.W., Miller M.C., 1997, *ApJ*, 479, 347
 Rogers F.J., Iglesias C.A., 1994, *Science*, 263, 50
 Romani R.W. 1987, *ApJ*, 313, 718
 Rutledge R.E., Bildsten L., Brown E.F., Pavlov G.G., Zavlin V.E., 2002, *ApJ*, 559, 1054
 Shibano Yu.A., Zavlin V.E., 1995, *Astron. Lett.*, 21, 3
 Shibano Yu.A., Zavlin V.E., Pavlov G.G., Ventura J., 1992, *A&A*, 266, 313
 Shibano Yu.A., Pavlov G.G., Zavlin V.E., Qin L., Tsuruta S., 1995, in *Proc. 17-th Texas Symposium on Relativistic Astrophysics*, eds. H. Bohringer, G. Morfill, & J. Trümper, Ann. NY Acad. Sci. 759 (New York), p.291
 Tsuruta, S., 1964, Ph.D. Thesis, Columbia Univ., N.Y.
 Walter F.M., Matthews L.D., 1997, *Nature*, 389, 358
 Werner K., Deetjen J., 2000, in *Pulsar Astronomy — 2000 and Beyond*, eds. M. Kramer, N. Wex & R. Wielebinski, ASP Conf. Ser., 202, 623
 Zane S., Turolla R., Stella L., Treves A., 2001, *ApJ*, 560, 384
 Zavlin V.E., Pavlov G.G., 1998, *A&A*, 329, 583
 Zavlin V.E., Shibano Yu.A., Pavlov G.G., 1995a, *Astron. Lett.*, 21, 149
 Zavlin V.E., Pavlov G.G., Shibano Yu.A., Ventura J., 1995b, *A&A*, 297, 441

Zavlin V.E., Pavlov G.G., Shibano Yu.A., 1996, A&A, 315,
141

Zavlin V.E., Pavlov G.G., Trümper J. 1998, A&A, 331, 821

Zavlin V.E., Trümper J., Pavlov G.G. 1999, ApJ, 525, 959

Zavlin V.E., Pavlov G.G., Sanwal D., Manchester R.N.,
Trümper J., Halpern J.P., Becker W., 2002, ApJ, 569, 894